

XBT data collected along the Southern Ocean “chokepoint” between New Zealand and Antarctica, 1994-2024

Giuseppe Aulicino^{*,1,2}, Antonino Ian Ferola^{1,3}, Laura Fortunato¹, Giorgio Budillon^{1,4}, Pasquale Castagno^{4,5}, Pierpaolo Falco^{4,6}, Giannetta Fusco^{1,4}, Naomi Krauzig^{4,6}, Giancarlo Spezie^{1,4}, Enrico Zambianchi^{4,6}, Yuri Cotroneo^{*,1,4}

¹ Dipartimento di Scienze e Tecnologie, Università degli Studi di Napoli “Parthenope”, Napoli, 80143, Italy

² Istituto di Scienze Polari, Consiglio Nazionale delle Ricerche, Bologna, 40129, Italy

³ European Space Agency, Frascati, 00044, Italy

⁴ Consorzio Nazionale Interuniversitario per le Scienze del Mare (CoNISMa), Roma, 00196, Italy

⁵ Dipartimento di Scienze Matematiche e Informatiche, Scienze Fisiche e Scienze della Terra, Università degli Studi di Messina, 98122, Italy

⁶ Dipartimento di Scienze della Vita e dell’Ambiente, Università Politecnica delle Marche, Ancona, 60131, Italy

⁷ Dipartimento di Scienze della Terra, Sapienza Università di Roma, Roma, 00185, Italy

* Correspondence to: Giuseppe Aulicino (giuseppe.aulicino@uniparthenope.it); Yuri Cotroneo (yuri.cotroneo@uniparthenope.it)

Abstract. This study presents the water column temperature data collected during several cruises on board the *Italica*, *Araon* and *Laura Bassi* research vessels, in the framework of the Climatic Long-term Interaction for the Mass balance in Antarctica (CLIMA), Southern Ocean Chokepoints Italian Contribution (SOChIC), and Marine Observatory of the Ross Sea (MORSea) projects, funded by the Italian National Antarctic Research Program (PNRA). Data were collected between New Zealand and the Ross Sea during the austral summers from 1994/1995 to 2023/2024. Across this chokepoint of the Antarctic Circumpolar Current, XBT Sippican T7 probes were launched with a regular 20 km sampling, providing temperature profiles with a vertical resolution of 65 cm and a maximum nominal depth of 760 m. All temperature profiles underwent a rigorous quality control, including a general malfunctioning verification, the removal of spikes, the consistency check of adjacent profiles, the comparison to regional oceanographic features and satellite altimetry observations, and a final visual check by operator. Data quality checks led us to discard about 12% of acquired XBT measurements. This dataset contributes to the improvement of our understanding of Southern Ocean features, being highly valuable for studies focusing on climate variability, especially across the Antarctic Circumpolar Current and its fronts. Furthermore, we expect that the collected XBT data will serve as a useful tool for the calibration and validation of recent satellite observations and for the improvement of Southern Ocean oceanographic simulations.

1 Introduction

The temperature of the ocean is one of the key parameters identified by the Global Climate Observing System (GCOS) as being essential for climate studies (World Meteorological Organization, 2016). Together with salinity values, ocean temperatures are necessary to identify and trace the main water masses and monitor their evolution at different spatial and temporal scales.

On the larger scales, collecting oceanic temperature and salinity data is of paramount importance to the study of the global thermohaline circulation, which plays a pivotal role in Earth's climate system. The Southern Ocean (SO) plays a fundamental role in this circulation (Gille, 1994; Rintoul, 2018), as some of the global thermohaline circulation "engines" are located near the Antarctic coast, associated with polynya areas (Morales Maqueda et al., 2004; Aulicino & Wadhams, 2022; Falco et al., 2024). At smaller scales, temperature data can be used to describe the vertical structure of the ocean (e.g., the thermocline depth and its variability), to locate fronts between different water masses, determine the ocean heat content and volume transport, and to identify meso- and sub-mesoscale ocean dynamics.

The main current in the SO is the Antarctic Circumpolar Current (ACC), which is its primary source of heat, nutrients and momentum (Sokolov & Rintoul, 2009a, 2009b). The ACC is one of the largest currents on the planet, flowing from west to east and isolating the Antarctic continent, which makes it strongly dependent on the SO conditions. Additionally, the Antarctic ecosystem is very fragile and temperature-dependent, which highlights the importance of monitoring physical changes in the ocean that surrounds it (Convey & Peck, 2019). Therefore, monitoring the SO and its temperature is essential for improving our knowledge of the processes driving the Antarctic variability and the global climate balance (Rintoul, 2018; Armour et al., 2016).

Despite its importance, SO has consistently faced a scarcity of in situ observations due to its remote location and the extreme weather conditions, which often hinder research activities to be carried out on site. The measurements are further limited by the seasonal sea ice presence that inhibits the navigation and the data collection. Additionally, in situ data collection is often conducted with instruments and probes used from ships travelling at their normal speed (e.g., Expendable BathyThermographs – XBT), without the possibility to perform classical full depth CTD casts that require ship stops. The advent of the international ARGO program increased significantly the number of hydrographic observations available in the SO throughout all seasons (Roemmich et al., 2022). However, Lagrangian floats do not allow the collection of information along repeated monitoring lines.

Accordingly, many steps have been taken over time to obtain ocean temperature data through remote sensing. Satellite data provide valuable insights about the upper ocean, especially when considering

that the surface layer is closely related to fundamental phenomena (e.g., ocean-atmosphere physical and biogeochemical interactions, fronts, currents, meanders, eddies) impacting the large-scale circulation and the meso- and small-scale characteristics of the ocean (e.g., McGillicuddy, 2016; Cotroneo et al., 2016; Seo et al., 2023). Additional information about the water column can also be retrieved from numerical models (e.g., Downes et al., 2015) and 3D reconstructions inferred through machine learning and statistical techniques applied to satellite observations, such as sea surface temperature (e.g., Buongiorno Nardelli et al., 2020). Nonetheless, in situ measurements are indispensable for achieving the necessary precision and depth coverage. In addition, they provide critical ground-truth for the calibration and validation of satellite retrievals of surface variables, and the improvement of data acquisition algorithms (Aulicino et al., 2022). It is therefore evident that the collection of in situ data is essential for monitoring ocean temperature.

The Global Ocean Observing System (GOOS) Ship Of Opportunity Program (SOOP), and the related Ship of Opportunity Program Implementation Panel (SOOPIP), address scientific and operational (standardization, maintenance, and advancement of the instruments and techniques) goals, respectively, to building a sustained ocean observing system, e.g., supplementing dedicated research vessels in the collection of upper ocean in situ XBT data through the use of ships that are already traversing the world's oceans (Legler et al., 2015; Goni et al., 2019).

In this scenario, the University of Naples Parthenope has been taking part since 1994 in the organization and execution of several oceanographic campaigns along the PX36 monitoring line in the Pacific sector of the SO, i.e., between New Zealand and the Ross Sea, in the framework of the Italian National Antarctic Research Program (PNRA). During each expedition, XBT launches were carried out, collecting ocean temperature data from surface to a maximum of about 760m depth (Falco et al., 2022). This study presents the collected XBT dataset, which significantly contributes to the accessibility of extensive ocean temperature data.

In this paper, the methodologies used for data collection and quality control (QC) are described in Section 2; the results and the discussion are reported in Section 3; the data record details and the conclusions are summarized in Section 4.

101 **2 Data and methods**

102 **2.1 The XBT dataset**

103 An XBT system is composed of several key components: an expendable ballistic probe that descends
104 into seawater; a data acquisition device that records an electrical signal and converts it into usable
105 numerical data (with the support of a computer unit); a double copper wire that connects the falling
106 probe to the acquisition device (Goni et al., 2019; Parks et al., 2022; Simoncelli et al., 2024). As the
107 probe descends through the water column, temperature measurements are acquired using a Negative
108 Temperature Coefficient (NTC) thermistor mounted on the probe zinc nose, which alters its resistance
109 in response to the seawater temperature it comes into contact with. The insulated copper wire is
110 unwound simultaneously by two spools, i.e., clockwise on the ship and counterclockwise in the falling
111 probe. This technique decouples the XBT vertical descent through the seawater from the ship
112 translational motion (Simoncelli et al., 2024). Data recording continues until the wire breaks or the
113 recording is terminated by the operator. The depth associated with a temperature measurement is not
114 measured directly because XBT probes do not contain pressure sensors. Instead, depth is estimated
115 using a phenomenological Fall Rate Equation (FRE). In our final data products, depth calculated from
116 the manufacturer's original FRE coefficients as well as corrected depths recommended by Hanawa et
117 al 1995 and Cheng et al 2014 are provided. These coefficients, along with details about the data
118 acquisition systems, are typically included in the metadata associated with each XBT cast.

119 The uncertainties on temperature and pressure values make the XBT probe accuracy be generally
120 rated to $\pm 0.10^{\circ}\text{C}$ (Parks et al., 2022), although differences can be retrieved depending on the
121 manufacturer and the manufacturing date of different devices (Cowley et al., 2013). Consequently,
122 some crucial information should be always provided with any XBT dataset for subsequent optimal
123 use of the measurements, including a complete description of the system characteristics in the
124 metadata (e.g., probe type, fall rate coefficients, data originator, platform).

125 We present here the dataset of water column temperatures collected in the Pacific sector of the
126 Southern Ocean through XBT casts during several research cruises on board the Italian research
127 vessels “Italica” and “Laura Bassi” and the Korean icebreaker “Araon” (see Table 1). These activities
128 were carried out in the framework of the Italian PNRA by several scientific projects, e.g., Climatic
129 Long-term Interaction for the Mass balance in Antarctica (CLIMA), Southern Ocean observing
130 system and Chokepoints Italian Contribution (SOChIC) and Marine Observatory in the Ross Sea
131 (MORSea).

132 The XBT casts were carried out during the austral summers between 1994/1995 and 2023/2024,
133 mainly in January and February (Figure 1), using Sippican T7 probes providing temperature profiles
134 with a vertical resolution of 65 cm and a maximum nominal depth of 760 m. Only during the

1994/1995 (PNRA_X) and 1995/1996 (PNRA_XI) cruises some Sippican T5 probes were used, reaching a maximum depth of 1830 m, as reported in the campaign metadata information (Table 2). The majority of transects were completed in 5-6 days and provide a synoptic picture of the thermal structure of the upper SO across its Pacific Sector (Figure 2). A regular 20 km sampling interval was adopted with occasional increased sampling frequency over the main frontal regions of the ACC.

Table 1. List of scientific cruises included in this dataset carried out between November 1994 and January 2024

Cruise name	R/V	Start date	End date	Latitude	Longitude
PNRA_X	ITALICA	03 November 1994	02 March 1995	47.00 - 74.99°S	172.02°E - 175.90°W
PNRA_XI	ITALICA	07 January 1996	18 February 1996	48.66 - 72.01°S	173.56°E - 179.79°E
PNRA_XII	ITALICA	26 January 1997	19 February 1997	46.17 - 74.69°S	166.24°E - 179.82°E
PNRA_XIII	ITALICA	23 November 1997	06 March 1998	46.25 - 72.71°S	171.39°E - 179.43°W
PNRA_XIV	ITALICA	05 January 1999	11 January 1999	48.07 - 69.00°S	173.70°E - 178.55°E
PNRA_XV	ITALICA	07 January 2000	18 February 2000	49.17 - 69.83°S	173.13°E - 178.41°E
PNRA_XVI	ITALICA	06 January 2001	26 February 2001	48.75 - 75.94°S	170.59°E - 179.72°E
PNRA_XVII	ITALICA	24 December 2001	31 December 2001	48.50 - 69.30°S	160.39°E - 178.01°E
PNRA_XVIII	ITALICA	06 January 2003	11 January 2003	48.00 - 71.26°S	172.93°E - 177.47°E
PNRA_XIX	ITALICA	24 December 2003	28 December 2003	46.36 - 66.17°S	173.81°E - 179.99°E
PNRA_XX	ITALICA	01 January 2005	06 January 2005	48.03 - 70.49°S	174.22°E - 178.38°E
PNRA_XXI	ITALICA	01 January 2006	04 January 2006	48.03 - 66.50°S	174.59°E - 179.93°E
PNRA_XXII	ITALICA	05 February 2007	10 February 2007	47.23 - 71.99°S	170.86°E - 174.26°E
PNRA_XXIII	ITALICA	16 January 2008	21 January 2008	47.50 - 68.99°S	174.18°E - 178.63°E
PNRA_XXV	ITALICA	25 January 2010	29 January 2010	46.38 - 70.00°S	173.63°E - 178.00°E
PNRA_XXVII	ITALICA	13 January 2012	19 January 2012	47.85 - 65.96°S	172.03°E - 176.54°E
PNRA_XXVIII	ARAON	24 January 2013	06 February 2013	47.20 - 68.5°S	158.30°E - 177.00°E
PNRA_XXIX	ITALICA	30 December 2013	18 February 2014	48.01 - 78.83°S	167.07°E - 175.84°W
PNRA_XXX	ARAON	02 January 2015	10 January 2015	47.99 - 73.22°S	157.02°E - 173.81°E
PNRA_XXXI	ITALICA	16 January 2016	28 January 2016	47.49 - 72.40°S	171.56°E - 175.00°E
PNRA_XXXII	ITALICA	31 December 2016	05 January 2017	48.01 - 68.77°S	174.09°E - 179.85°W
PNRA_XXXIV	ARAON	08 February 2019	12 February 2019	47.99 - 69.75°S	166.79°E - 170.87°E
PNRA_XXXV	LAURA BASSI	07 January 2020	12 January 2020	48.01 - 69.25°S	172.97°E - 178.84°E
PNRA_XXXVI	LAURA BASSI	25 December 2020	02 January 2021	46.96 - 73.39°S	172.82°E - 175.89°E
PNRA_XXXVII	LAURA BASSI	08 January 2022	26 January 2022	47.54 - 76.35°S	171.20°E - 177.58°W
PNRA_XXXVIII	LAURA BASSI	06 January 2023	12 January 2023	46.56 - 72.27°S	169.40°E - 178.70°E
PNRA_XXXIX	LAURA BASSI	07 January 2024	12 January 2024	48.20 - 70.00 °S	166.30 °E – 176.40°E

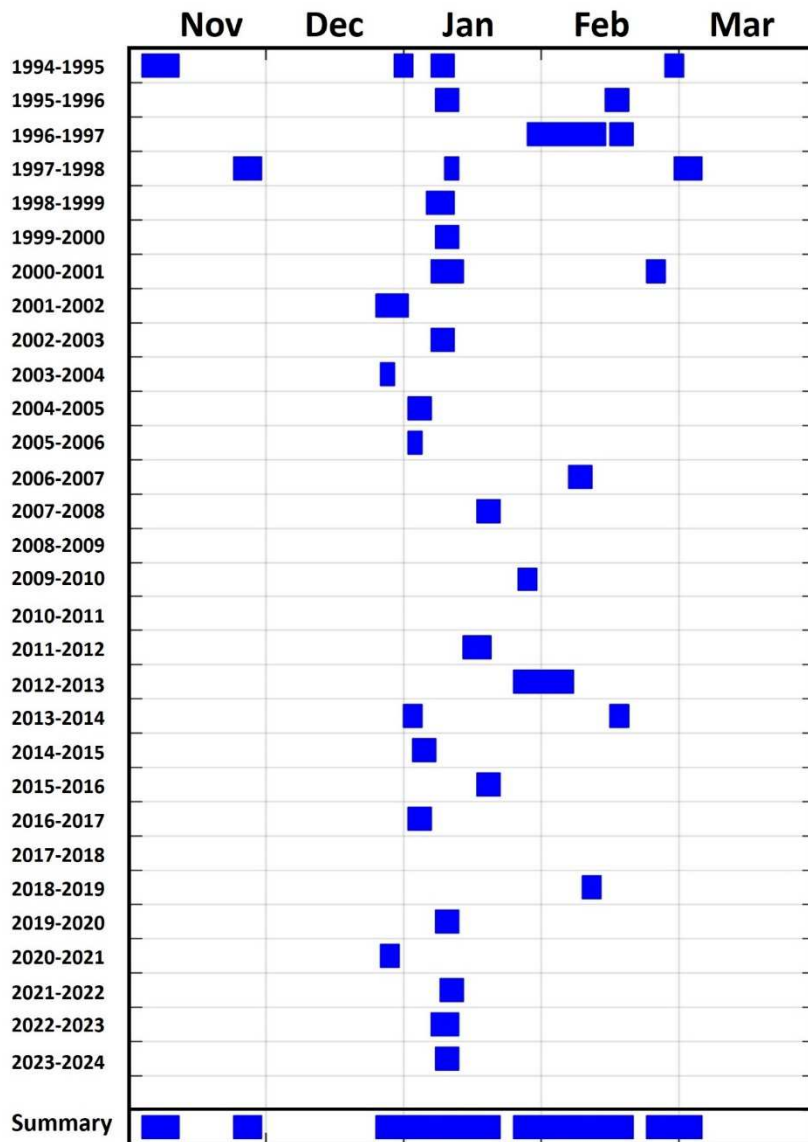
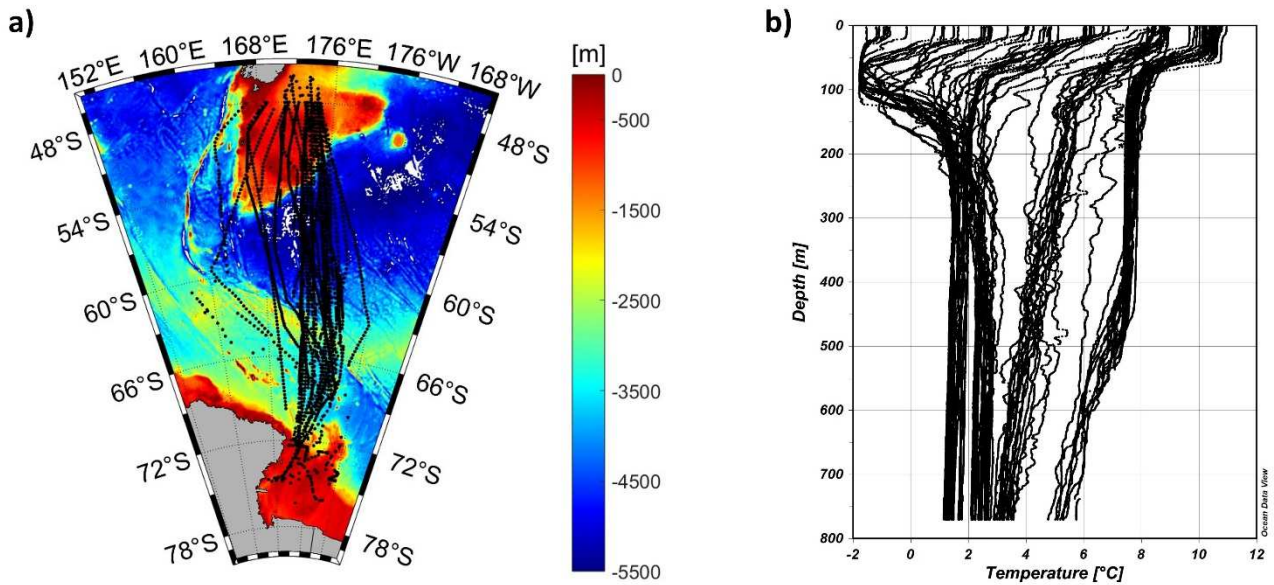


Figure 1. Temporal distribution of the oceanographic campaigns conducted along the New Zealand-Antarctica “chokepoint” between 1994 and 2024.

Table 2. Characteristics of the different XBT probes used in this study: nominal depth guaranteed by Sippican; maximum ship speed suggested by Sippican for an optimal drop; amount of ZAMAK (a zinc-based alloy enriched with aluminium, magnesium, and copper), copper and plastic for each probe type (adapted from Simoncelli et al., 2024)

Probe type	Max rated depth (m)	Max ship speed (knots)	ZAMAK (kg)	Plastic (kg)	Copper (kg)
Sippican T5	1830	6	0.613	0.125	0.357
Sippican T7	760	15	0.576	0.052	0.240



156

157 **Figure 2. a)** Map of the Southern Ocean area between New Zealand and Antarctica. The black dots represent the position
158 of all XBT launches carried out between December 1994 and January 2024. **b)** An example of temperature vertical profiles
159 collected through XBT across the New Zealand – Ross Sea chokepoint during the XXXV Italian Antarctic Expedition.

160

161

162

2.2 Quality Control

163 Various types of malfunctions can affect XBT measurements and result in inaccurate temperature
164 readings within the temperature profile. These faults can appear as a spike in a single recorded value
165 or affect the temperature across a range of depths. Moreover, some issues can create errors that mimic
166 real phenomena, such as temperature inversions or fronts (Parks et al., 2022; Cowley and Krummel,
167 2022). Sometimes, profiles can be corrected by deleting or filtering sections of the original data.
168 However, an accurate quality control procedure must be implemented before any data is discarded or
169 manipulated. Additionally, a flagging scheme is generally applied to provide XBT dataset users with
170 quality indicators of the oceanographic data.

171 Quality flags (QFs) are essential for enabling users to filter the XBT dataset according to the specific
172 quality requirements for the intended use. Several flagging scheme exist in agreement with
173 recommendations provided by the Intergovernmental Oceanographic Commission of UNESCO
174 (IOC, 2013). In this study we follow the suggestions provided by the Global Temperature and Salinity
175 Profile Program (GTSP) of the NOAA-NCEI (<https://www.ncei.noaa.gov/products/global-temperature-and-salinity-profile-programme>) resulting in the flagging scheme summarized in Table
176 3 for indicating the quality of each temperature and depth data point.
177

178

179 **Table 3.** The Quality Flags (QF) assigned to the XBT data

QF	Quality	Description
0	No QC	No quality control has been performed on this data.
1	Good data	The data is good. No malfunctions have been identified and consistency with real phenomena has been verified.
2	Probably good data	Minor malfunctions present which are small or correctable without affecting overall data quality. Some features (probably real) are present but these are unconfirmed.
3	Probably bad data	Data are suspect and present unusual features which are inconsistent with real phenomena, Data remains potentially correctable.
4	Bad data	The data appears erroneous. Evident errors are identified and there is no likelihood of correction.

180

181

182 The assignment of QFs is the result of a series of quality control (QC) tests for both temperature and
183 depth data which are used to get a reliable quality check of the temperature measurements collected
184 through our XBTs and of the retrieved depths. Results of each test allowed to insert the relative flag
185 to the corresponding measurement according to the scheme shown in Table 3. QF=1 is assigned when
186 all the tests pass and QF=4 when at least one test fails. For temperature, more detailed checks are
187 performed, including a final visual check, allowing us to introduce QF=2 and QF=3 for probably
188 good and probably bad data, respectively (as detailed below).

189 Overall, the QC procedures applied to our dataset follow recommendations previously suggested by
190 NOAA, developed and refined in the last three decades (Bailey et al., 1994; Daneshzadeh et al., 1995;
191 Cowley and Krummel, 2022; Parks et al., 2022; Tan et al., 2023). These procedures include several
192 steps undertaken in a top-down manner, as temperature data are measured from the surface down,
193 and faults that occur at a given depth may impact on deeper data (Parks et al., 2022).

194 First, each XBT profile was tested for invalid metadata information, such as the correct time, cast
195 position and any other possible operator errors, using a sequence of independent checks. All identified
196 errors in date and time were corrected accordingly, with the support of the XBT launch log sheets
197 provided by operators on board. No errors were found concerning the position of the casts after the
198 comparison of latitudes and longitudes against gridded GEBCO 2 x 2 minutes bathymetry (GEBCO
199 Compilation Group, 2023). The check of unrealistic positions was also performed using the
200 calculation of vessel speed from profile date and time and an upper general threshold of 20 knots
201 (since most of the launches are realized by ships travelling in the range of 10/15 knots). Additionally,
202 the depth values of each XBT profile were compared to the last good depth value provided by the
203 operators (QF=1 is assigned to shallower depth values, otherwise they are flagged as QF=4).

Then, all the vertical temperature profiles were checked for nominal maximum depth (760 m), and carefully inspected to identify malfunctions, coherence to regional oceanographic features, drop-to-drop consistency along the cruise track, and presence of unusual features. In this context, the main difficulty is usually found in distinguishing a common malfunction from a regional oceanographic feature (i.e., unexpected increase of temperature southward or along the water column). Consequently, unusual features were cross-validated by comparison to repeated (within 15 minutes) or neighbouring profiles from the same voyage and eventually to available Austral summer ARGO observations over the study area. To this aim, we took again advantage of XBT launch log sheets, in which operators notified any instrument malfunctions, adverse weather conditions, sea ice presence and local bottom depth. In particular, the bottom depth was relevant to constraining XBT data profiles at the right depth, especially when approaching shallow waters (QF=1 is assigned to values shallower than bottom depth, otherwise they are flagged as QF=4). When the log sheet was unavailable, we relied instead on the GEBCO 2 x 2 minutes bathymetry (GEBCO et al., 2023), which closely corresponded to the in situ reported depths over the area and period of study. Additionally, a gross filter was applied to all the XBT profiles using temperature ranges that vary on four vertical layers, as reported in Table 4. The ranges were defined through the use of ARGO data collected in the study area between 2004 and 2023. QF=4 was applied to data exceeding the thresholds of $\pm 0.5^{\circ}\text{C}$.

Table 4. Temperature ranges applied to XBT profiles, defined in four levels.

Depth range (m)	Temperature minimum ($^{\circ}\text{C}$)	Temperature maximum ($^{\circ}\text{C}$)
0 - 100	-1.866	14.698
100 - 250	-1.865	11.093
250 - 500	0.068	8.717
500 - 760	0.826	8.266

Several studies assess that the XBT measurements near the sea surface may be considered unreliable due to the stabilization of motion and thermal adaptation to the surrounding environment (e.g. Bailey et al., 1994; Cowley and Krummel, 2022; Simoncelli et al., 2024). They also suggest that the first acceptable value is at about 4 m depth and that the data user must be carefully informed in order to exclude suspect surface values from scientific analyses. Here, we opted for providing all the original measurements annotating their quality, as resulting from a dedicated test on the initial part of each profile. This test calculates the differences between the value recorded at time $t = 0.6$ s (about 4 m depth) and shallower measurements, classifying them based on the standard uncertainty on

233 temperature attributable to an XBT probe (0.10 °C) as a metric (Simoncelli et al., 2024). Therefore,
234 temperature data are assigned QF=1 if the difference is less than or equal to standard deviation (std);
235 QF=2 if it is comprised between std and 2*std; QF=3 if it is comprised between 2*std and 3*std; and
236 QF=4 if it is higher than 3*std.

237 Then, the XBT profiles were examined for the presence of spikes, unrealistic oscillations and unusual
238 gradients in temperature data, as well as sharp variations toward negative or higher values, which
239 could be caused by copper wire breaks. Data are mostly flagged as good (QF=1) or bad (QF=4)
240 values. Nonetheless, suspect data are compared with neighbouring profiles and ARGO climatology
241 over the study area (obtained from products available at [https://www.coriolis.eu.org/Data-](https://www.coriolis.eu.org/Data-Products/Data-selection)
242 [Products/Data-selection](https://www.coriolis.eu.org/Data-Products/Data-selection)), eventually assigning QF=1, QF=2 and QF=3 attributes. For example, QF=2
243 is used when an XBT profile presents a step-like feature that is not confirmed by a neighbouring
244 profile but is consistent with similar features previously observed in the study region. QF=3 is used,
245 instead, when XBT values exhibit suspect temperature values that cannot be confirmed by a
246 neighbouring profile and occur in areas where there is no evidence of mesoscale structures (e.g.,
247 eddies or fronts).

248 Nevertheless, an increase or decrease in temperature over large depth ranges compared to
249 neighbouring profiles, can be also associated to an eddy, a frontal area or an intense current system.
250 Therefore, QF=1 is applied when repeated profiles showing similar temperatures or archive data can
251 confirm the feature. The larger scale description of ocean dynamics obtained through satellite
252 altimetry was also used for controversial results to identify the presence of eddies and frontal systems
253 affecting the temperature data.

254 However, some profiles might exhibit anomalous features that the described QC procedure could not
255 detect as erroneous values. Therefore, an additional visual check was carried out for each individual
256 cruise track and each vertical temperature profile to verify the assigned QF=2 and QF=3 flags and
257 identify any residual anomalies in the positioning of the XBT launches or outliers in the data
258 collection. This control was performed using the Ocean Data View (ODV) software (Schlitzer, 2023).
259 Overall, the entire QC led us to discard about 12% of acquired XBT observations, which were flagged
260 as bad or probably bad data (Figure 3).

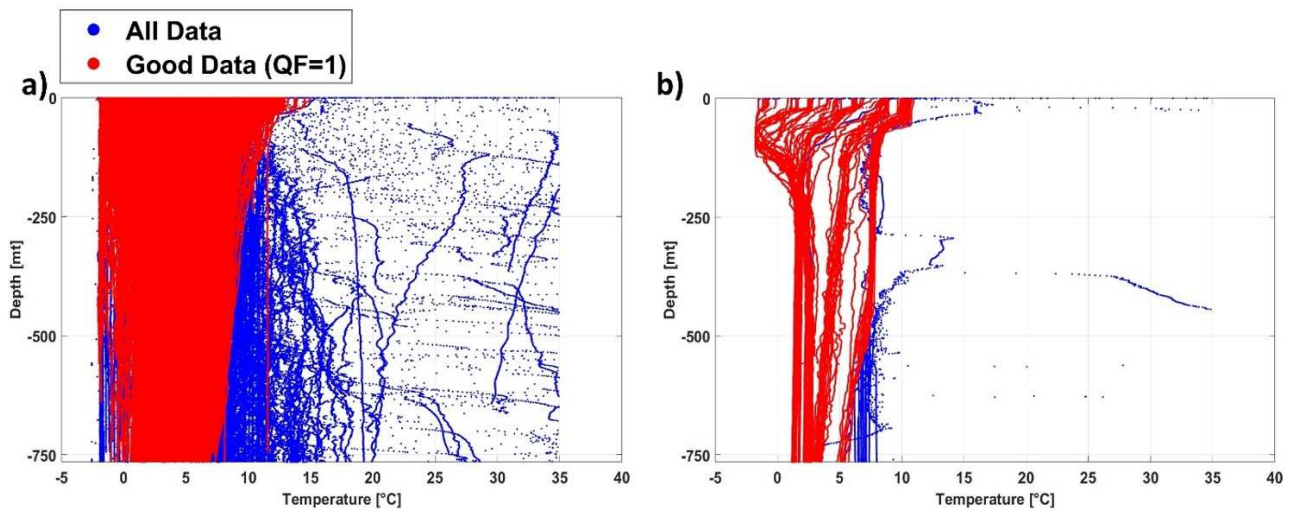


Figure 3. a) XBT observations collected between December 1994 and January 2024 over the New Zealand – Ross Sea chokepoint before (blue) and after (red) the quality check; **b)** An example of the quality check on the XBT data collected during the PNRA_XXXV cruise.

2.3 XBT data biases correction

Previous studies assessed that temperature biases and depth errors, due to inaccurate time conversion to depth through FRE, may affect XBT observations (e.g., Gouretski and Reseghetti, 2010; Cowley et al., 2013). Although a full comprehension of the origins of these issues is still pending, several experiments tried to quantify this bias by comparing XBT profiles with co-located CTD observations, demonstrating that XBT temperatures are usually warmer than reality (Gouretski and Reseghetti 2010; Cheng et al., 2014). Different possible causes of biases emerged, including mechanical (e.g., probe type, manufacturer, year), external (e.g., launch height, meteo-marine conditions) and electrical (e.g., thermistor, wire) factors (Seaver and Kuleshov 1982; Green, 1984; Reverdin et al. 2009). Additionally, a decrease in fall rate was observed in cooler waters because of increased viscosity (Gouretski and Reseghetti 2010), making FRE corrections in the Southern Ocean extremely important (Cheng et al., 2014).

To address these problems, several correction schemes have been proposed over the past few decades. A comprehensive list of related papers is available at <https://www.ncei.noaa.gov/products/xbt-corrections>. Taking advantage of more than 220,000 co-located XBT-CTD pairs, Cheng et al. (2014) examined and compared existing methodologies, proposing a new correction scheme for historical XBT data for nine independent probe-type groups. Their study confirmed that depth error and pure temperature bias are temperature-dependent and may be influenced by the data acquisition and recording system. Moreover, the resulting scheme also considers that some biases affecting the XBT-

285 derived temperature profiles vary with manufacturer/probe type and have been shown to be time
286 dependent, and that depth correction varies with depth (Cheng et al. 2016).
287 In our dataset, we apply this methodology, which includes corrections for both temperature and depth
288 values based on calendar year, water temperature, and probe type, to provide bias-corrected XBT
289 measurements (Cheng et al., 2014). To this aim, we use the Hanawa et al. (1995) coefficients (i.e.,
290 $A=6.691$, $B=0.00225$) in the Fall Rate Equation $D(t) = At - Bt^2$ to derive temperature measurement
291 depths starting from the time elapsed since the probe's release and, consequently, the bias-corrected
292 depth and temperature values. A full description of the methodology is available at
293 <https://www.ncei.noaa.gov/products/xbt-corrections> (see CH Correction Method); the update tables
294 of the applied coefficients are available at
295 http://www.ocean.iap.ac.cn/ftp/images_files/CH14_description/CH14_table1_update2023.txt and
296 http://www.ocean.iap.ac.cn/ftp/images_files/CH14_description/CH14_table2_update2023.txt.

299 **3. Results and discussion**

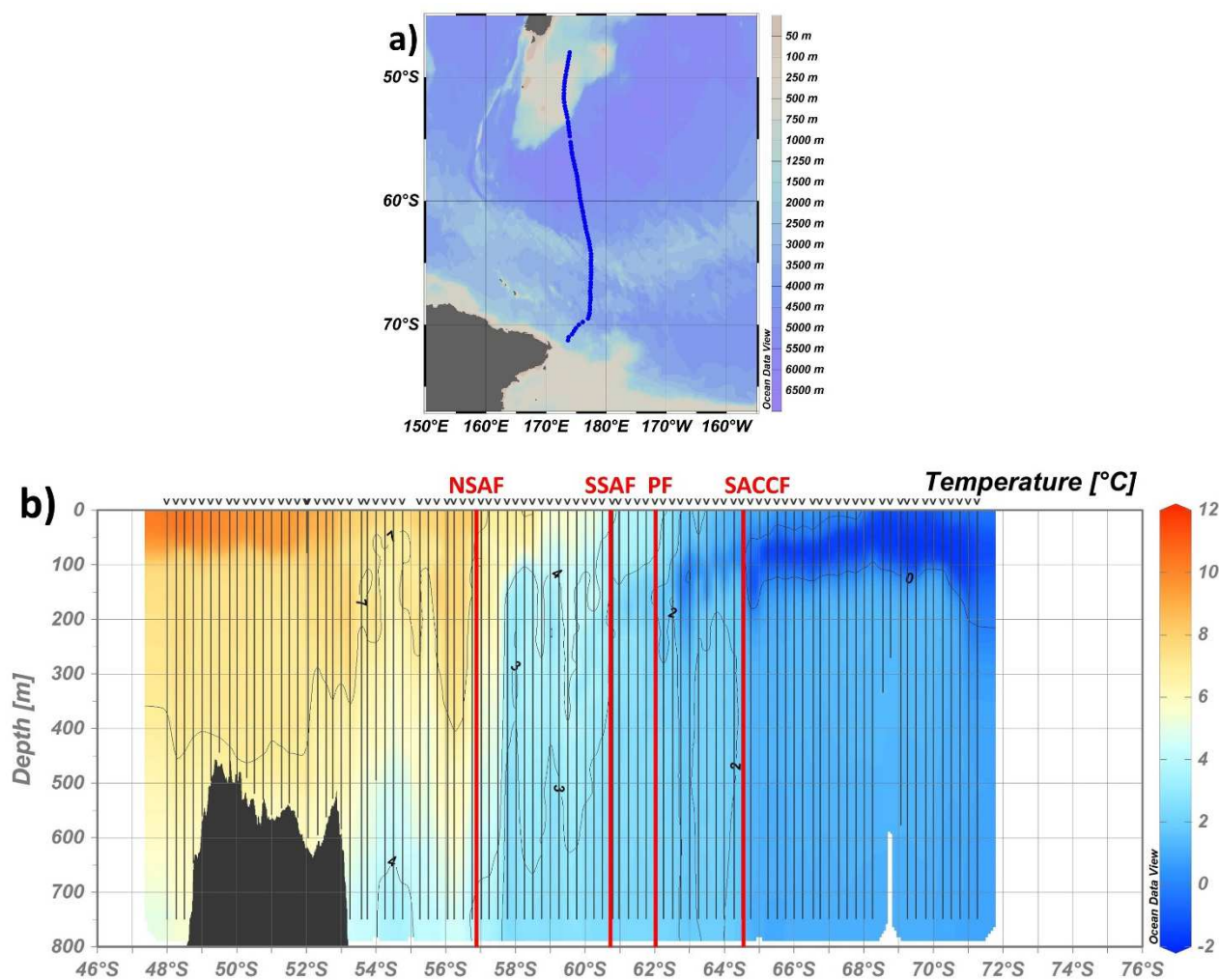
300 We believe this exceptional temperature dataset provides a valuable reservoir of high-resolution,
301 independent, and trustworthy information. The dataset assumes notable significance, representing an
302 extensive temporal series of data collected nearly every austral summer over the last 30 years, within
303 the same oceanic sector of the SO and along the same monitoring transect (PX36). We exploited this
304 information to provide 36 vertical sections of the ocean temperature, from the surface to about 800 m
305 depth, along the New Zealand–Antarctica “chokepoint”. Figures representing the latitudinal sections
306 of corrected XBT temperatures during each leg are available in the supplementary information
307 (Figures S1-S36) .

308 The repeated temperature sections significantly enhance our understanding of ACC fronts and their
309 evolution over the last three decades. A first application of the dataset is shown in Figure 4 where
310 XBT observations collected during the PNRA_XVIII expedition are used for the identification of the
311 main ACC fronts positions: Northern Sub Antarctic Front (NSAF); Southern Sub Antarctic Front
312 (SSAF); Polar Front (PF); Southern Antarctic Circumpolar Current (sACCF). The criteria used for
313 identifying the fronts (Table 5) follow Budillon and Rintoul (2003), which compiles several
314 hydrographic definitions (Botnikov, 1963; Belkin, 1990; Orsi et al., 1995; Rintoul et al., 1997). The
315 Southern boundary of the ACC, usually described as the maximum southern extent of vertical
316 maximum of $T > 1.5^{\circ}\text{C}$ at about 200 m (Orsi et al., 1995), is not described in this sector as its position
317 is coincident with the sACCF position in most of the available temperature sections.

318

319

320



321

322

323

324

325

326

327

328

Figure 4. **a)** Map of the position (blue dots) of all XBT launches carried out during the PNRA_XVIII expedition along the New Zealand–Antarctica “chokepoint” (6-11 January 2003). **b)** Temperature vertical section from XBT data in a) in which the vertical black lines represent the XBT casts and the red ones the ACC main fronts positions: Northern Sub Antarctic Front (NSAF); Southern Sub Antarctic Front (SSAF); Polar Front (PF); Southern Antarctic Circumpolar Front (SACCF). The black mask represents the bathymetry. Figures are produced through Ocean Data View.

Table 5. Criteria for front definitions (Adapted from Budillon & Rintoul, 2003)

Front	Definition	Reference
Southern Antarctic Circumpolar Current Front (sACCF)	$T > 1.8^{\circ}\text{C}$ along the Tmax at depth > 500 m, farther north; $T < 0^{\circ}\text{C}$ along the Tmin at depth < 150 m, farther south.	Orsi <i>et al.</i> 1995.
Polar Front (PF)	$T < 2^{\circ}\text{C}$ at 200 m, farther south.	Botnikov 1963, Orsi <i>et al.</i> 1995.
Subantarctic Front (SAF)	Maximum temperature gradient in the range $3\text{--}8^{\circ}\text{C}$ at 300 m.	Belkin 1990.
Northern Sub-Antarctic Front (NSAF)	Maximum temperature gradient in the range $4\text{--}7^{\circ}\text{C}$ at 300 m.	Rintoul <i>et al.</i> 1997.
Southern Sub-Antarctic Front (SSAF)	Maximum temperature gradient in the range $3\text{--}4^{\circ}\text{C}$ at 300 m.	Rintoul <i>et al.</i> 1997.

329

330
331
332
333
334
335
336
337
338
339
340
341
342
343
344
345
346
347
348
349
350
351
352
353
354
355
356
357
358
359

The ACC fronts positions retrieved through XBT data also serve as ground truth for the validation of those retrieved through satellite altimetry (e.g., Sokolov and Rintoul 2009a, 2009b; Graham et al., 2012; Chapman, 2017), thereby enhancing the identification process of fronts within the SO. This is highly desirable in regions significantly influenced by topographic steering, such as the area south of New Zealand, where the presence of the Campbell Plateau strongly affects the ACC path (Figure 5). To point out differences and similarities between ACC fronts positions identified through XBT and satellite observations, in Figure 5 we present a Sea Surface Height (SSH) map of the study area, averaged over the period covered by the temperature section in Figure 4 (about 7 days). To identify the ACC fronts from satellite data, we applied the SSH isolines methodology that associates a specific value of SSH with each front. For the selection of these values, we relied on previous studies (Sokolov and Rintoul 2007, 2009a, 2009b) proving that the multiple jets of ACC fronts are consistently aligned with streamlines identified by nearly constant circumpolar values of SSH contours.

Furthermore, ACC fronts exhibit instabilities that give rise to the generation of eddies. Eddies, characterized as vortices pervading the ocean, assume a pivotal role, particularly within the SO, contributing significantly to the transfer of heat, nutrients, and momentum (e.g., Chelton et al. 2011a; Falco and Zambianchi, 2011; Cotroneo et al., 2013; Trani et al., 2014; Rintoul, 2018; Menna et al., 2020). While altimetry proves valuable in gaining insights into surface eddy dynamics, it cannot provide information regarding vertical temperature variations within the eddy structure. Through the temperature sections derived from XBT data, we can discern the presence or absence of an eddy and get basic observations for the analysis of its heat content.

An example is provided in Figure 6 where we present the latitudinal section of temperatures observed during the return leg of the 2013-2014 Italian Antarctic expedition (PNRA_XXIX). This section shows the intrusion of a cold core eddy at about 53°S, next to the Campbell Plateau edge. The eddy is characterized by a maximum negative temperature anomaly (eddy's core) of about -4°C compared to the surrounding water. This negative anomaly results in the formation of a depression in the SSH, also detectable in satellite imagery. In the SSH map shown in Figure 7, the cold core eddy is identified as a closed circle of the blue isoline associated with the SSAF.

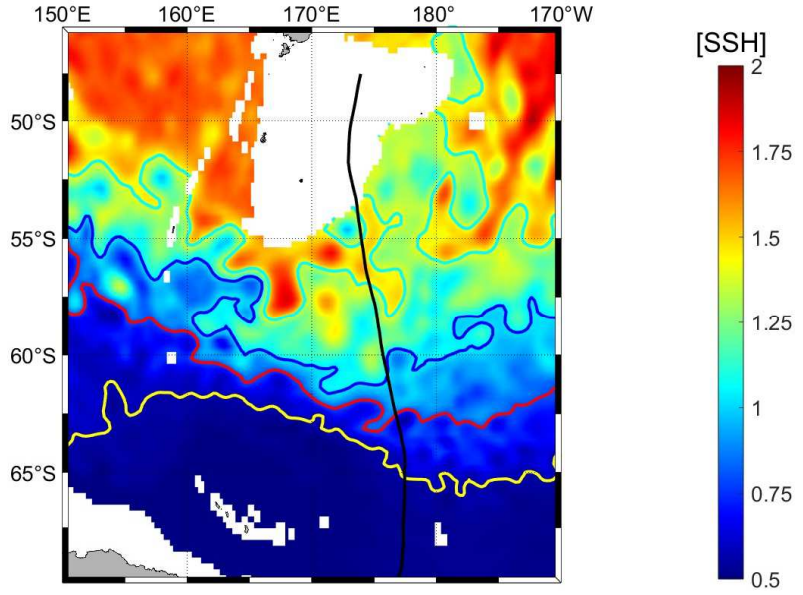
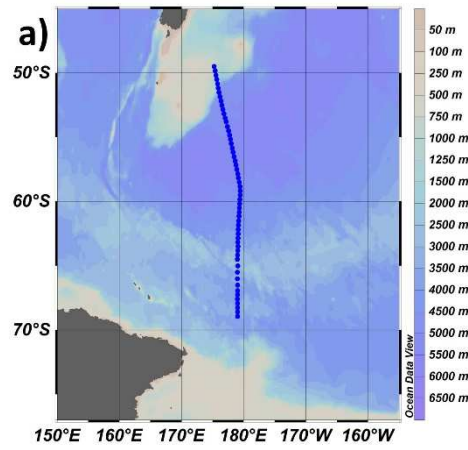


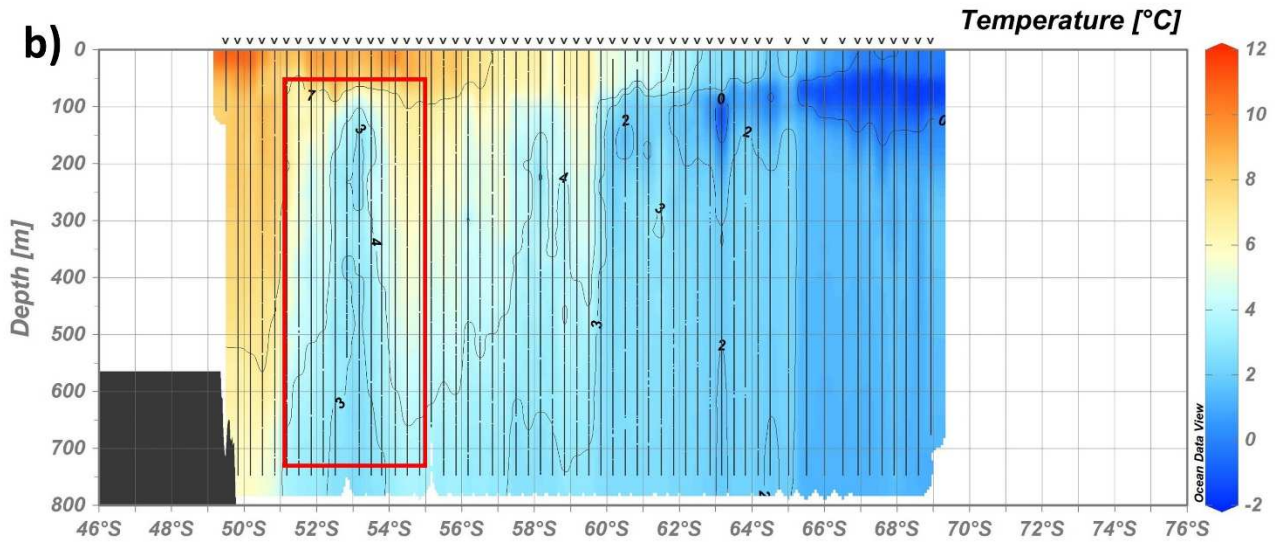
Figure 5. Altimetric map of SSH mediated throughout the PNRA_XVIII expedition along the PX36 monitoring line. Contours of different colours identify the position of the main fronts of the ACC retrieved through SSH: NSAF in cyan; SSAF in blue; PF in red and sACCf in yellow. White crosses represent the position of the fronts derived from XBT data. The ship's route is represented by the black line.

Generally, the combined use of in situ observations and satellite data is crucial as it prevents errors in front positioning and eddy identification. Strong horizontal temperature gradients, often linked to eddies, could be misinterpreted as ACC fronts. Similarly, this approach allows us to distinguish eddies from other mesoscale structures, a difficult task when relying only on altimetry. XBT and satellite information are also complementary in providing valid terms of comparison, at different temporal and spatial scales (XBT at fine-scale; altimetry at meso- and large-scale), for numerical model products representing ocean circulation and eddies dynamics (e.g., Chen X. et al., 2024; Chen Z. et al., 2024).

376



377



378

379

380

381

382

Figure 6. a) Map of the position (blue dots) of all XBT launches carried out during the PNRA_XXIX expedition along the New Zealand–Antarctica “chokepoint” (30 December 2013 – 18 February 2014). **b)** Temperature vertical section from XBT data in a) in which the vertical black lines represent the XBT casts and the red box identifies the position of an ACC’s cold core eddy. The black mask represents the bathymetry. Figures are produced through Ocean Data View.

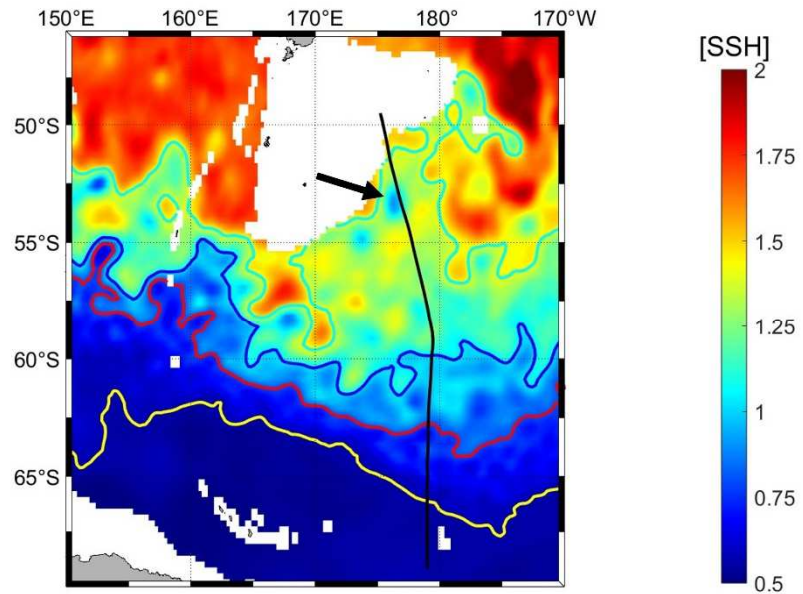


Figure 7. Altimetric map of SSH mediated throughout the PNRA_XXIX expedition along the PX36 monitoring line. Contours of different colours identify the position of the main fronts of the ACC retrieved through SSH: NSAF in cyan; SSAF in blue; PF in red and sACCf in yellow. White crosses represent the position of the fronts derived from XBT data. The ship's route is represented by the black line. The black arrow indicates the observed cold core eddy.

4. Data availability

The full XBT dataset presented here is publicly accessible as text format files at <https://doi.org/10.5281/zenodo.14848849> (Aulicino et al., 2025). Individual cruise data are also available through the National Oceanic and Atmospheric Administration (NOAA) National Centers for Environmental Information (NCEI) unrestricted repositories, as listed in Table 6. NCEI serves as the official archive for data, metadata, and products collected and provided by NOAA scientists. Additionally, NCEI hosts quality checked data from non-NOAA scientists, which must go through a scientific appraisal process before being accepted into the archive. For this reason, our XBT data underwent a thorough review and improvement process (see sections 2.2 and 2.3) prior to publication, resulting in the full dataset presented here, available through the Zenodo repository.

Each XBT file includes the main variables summarized in Table 7, the relative EMODNet-compliant metadata (i.e., about probe type, software, manufacturer, data originator, scientific project, platform, uncertainties, QF code), detailed information about the FRE coefficients used for temperature and depth bias correction described in section 2.3, and a short description of the dataset. The manufacturer FRE coefficients are also provided in the metadata, allowing anyone who wishes to recalculate the corrections in a different way than using Cheng et al. (2014).

One file is created for each research cruise. The naming convention is xbt_cruise, where cruise is the identification “cruise name” of the PNRA research expedition, as in Table 1. Please note that the format and labels of the provided XBT text files are ODV-compliant to facilitate ease of use. All the temperature sections presented in Figures 4, 6, and S1-S36, were realized using ODV software and applying consistent interpolation parameters. The adopted zonal interpolation is based on a spatial weighting model that incorporates three temperature profiles (a central reference profile, an upstream profile, and a downstream profile), considering a maximum influence range of 60 km along the zonal direction and 20 m along depth.

Additionally, a Python code for basic XBT data visualization is included in supplemental material S37 (such as shown for scatter plots of vertical temperature profiles and latitudinal temperature sections in Figures S38 and S39).

416

417 **Table 6.** XBT individual cruise data repository list

Data set	DOI	Reference
PNRA_X – 1st leg	https://doi.org/10.7289/v5rf5s9v	Cotroneo et al., 2018a
PNRA_X – 2nd leg	https://doi.org/10.7289/v53r0r5z	Cotroneo et al., 2018b
PNRA_XI	https://doi.org/10.7289/v5x065b9	Cotroneo et al., 2018c
PNRA_XII	https://doi.org/10.7289/v5kd1w6b	Cotroneo et al., 2018d
PNRA_XIII	https://doi.org/10.7289/v50863mf	Cotroneo et al., 2018e
PNRA_XIV	https://doi.org/10.7289/v5mg7mtc	Cotroneo et al., 2018f
PNRA_XV	https://doi.org/10.7289/v56d5r8p	Cotroneo et al., 2018g
PNRA_XVI	https://doi.org/10.7289/v5s75dpg	Cotroneo et al., 2018h
PNRA_XVII	https://doi.org/10.7289/v5ng4nzt	Cotroneo et al., 2018i
PNRA_XVIII	https://doi.org/10.7289/v5qz289c	Cotroneo et al., 2018j
PNRA_XIX	https://doi.org/10.7289/v5vq3113	Cotroneo et al., 2018k
PNRA_XX	https://doi.org/10.7289/v5vh5m45	Cotroneo et al., 2018l
PNRA_XXI	https://dx.doi.org/10.25921/hzcp-d813	Cotroneo et al., 2019
PNRA_XXII	https://doi.org/10.25921/c8bm-xh74	Cotroneo et al., 2018m
PNRA_XXIII	https://doi.org/10.25921/q29v-c980	Cotroneo et al., 2018n
PNRA_XXV	https://doi.org/10.7289/v50r9mmm	Cotroneo et al., 2017a
PNRA_XXVII	https://doi.org/10.7289/v54j0cbw	Cotroneo et al., 2017b
PNRA_XXVIII	https://doi.org/10.25921/9YTS-P771	Cotroneo et al., 2018o
PNRA_XXIX	https://doi.org/10.25921/220j-b370	Cotroneo et al., 2024a
PNRA_XXX	https://doi.org/10.25921/9ph6-c102	Cotroneo et al., 2024b
PNRA_XXXI	https://doi.org/10.25921/zf04-ch06	Cotroneo et al., 2024c
PNRA_XXXII	https://doi.org/10.25921/vvmp-rr55	Cotroneo et al., 2024d
PNRA_XXXIV	https://doi.org/10.25921/jeee-zf77	Cotroneo et al., 2024e
PNRA_XXXV	https://doi.org/10.25921/lysg-dw94	Cotroneo et al., 2024f
PNRA_XXXVI	https://doi.org/10.25921/aeg5-hw87	Cotroneo et al., 2024g
PNRA_XXXVII	https://doi.org/10.25921/3mmd-tj60	Cotroneo et al., 2024h

PNRA_XXXVIII	https://doi.org/10.25921/kte7-d058	Cotroneo et al., 2024i
PNRA_XXXIX	https://doi.org/10.25921/jc13-ek97	Cotroneo et al., 2024l

Table 7. Name and description of the main variables included in the XBT text files.

Name of variable	Unit	Description
Cruise		Cruise name
Station		Identifier number of XBT deployment
Type		Instrument type
Date	dd/mm/yyyy	Date of XBT deployment
Time	hh:mm	Time of XBT deployment
Latitude [degrees_north]	Decimal degrees	Latitude of XBT deployment
Longitude [degrees_east]	Decimal degrees	Longitude of XBT deployment
Bot. Depth [m]	Meters	Maximum depth reached by the XBT probe
Elapsed Time [s]	Seconds	Time elapsed since the release of the XBT probe
Depth 1 [m]	Meters	Depth derived from the elapsed time using the Manufacturer Fall Rate Equation Coefficients
Depth 2 [m]	Meters	Depth derived from the elapsed time using the Hanawa et al. (1995) Fall Rate Equation Coefficients
Depth 3 [m]	Meters	Depth 2 corrected following Cheng et al. (2014) with Hanawa et al. (1995) Fall Rate Equation Coefficients
Temperature 1 [°C]	Celsius degrees	Temperature measured by the XBT probe
Temperature 2 [°C]	Celsius degrees	Temperature corrected following Cheng et al. (2014) with Hanawa et al. (1995) Fall Rate Equation Coefficients
QF	0 – 4	Quality flags of XBT measurements

5. Conclusions

The SO is a key place for atmosphere–ocean physical and biogeochemical interactions at different spatial and temporal scales (Falco and Zambianchi, 2011; Cerrone et al., 2017a, b; Buongiorno Nardelli et al., 2017; Falco et al., 2024). However, despite their importance, processes in many areas of the SO are still poorly known due to the scarcity of in situ measurements. This is particularly true for the ACC region and its fronts, which are characterized by complex dynamics and intense eddy activity (Trani et al., 2011; Cotroneo et al., 2013; Frenger et al., 2015; Menna et al., 2020; Ferola et al., 2023). To fill this gap, all available measurements provide a significant contribution and should be shared within the oceanographic community.

To this goal, here we present 36 vertical sections of XBT ocean temperature data collected between New Zealand and the Ross Sea (PX36 line) during the Austral summers from 1994/1995 to 2022/2023. This dataset provides direct insights into the 0-800 m thermal characteristics of the Pacific sector of the SO and complements data sourced from observing networks, drifters, ARGO floats and glider fleets. It is also suitable to be combined with enhanced spatial and temporal scale remotely sensed observations and numerical simulations. This comprehensive dataset lays a robust foundation

for a nuanced analysis of the key mechanisms governing thermohaline circulation in the SO and for improving our knowledge of the physical and biogeochemical characteristics of the four-dimensional ocean.

The continuation of this XBT collection over time, in the framework of the Italian PNRA research expeditions to Antarctica, is particularly important due to the inherent challenges associated with data acquisition in the SO and promises an increasingly comprehensive and detailed understanding of thermal variations in this specific maritime region.

443

Author contributions. GA, YC and AIF conceived and designed the manuscript. GA, YC, PC, PF, GF, GB, NK, GS, EZ and AIF collected the measurements and organized the XBT dataset. GA, YC, LF and AIF carried out the quality control analyses. All authors analysed the achieved results, contributed to the writing, and approved the final manuscript.

Competing interests. The authors declare that they have no conflict of interest.

449

Acknowledgements. This study was made possible thanks to the contribution of the Climatic Long-term Interaction for the Mass balance in Antarctica (CLIMA), Southern Ocean Chokepoints Italian Contribution (SOChIC), Marine Observatory of the Ross Sea (MORSea), Effects of the east current on the Salinity variability in the Ross Sea (ESTRO), Physical and biogeochemical tracing of water masses at source areas and export gates in the Ross Sea and impact on the Southern Ocean (SIGNATURE) and Antarctic Circumpolar Current Eddies Survey and Simulations (ACCESS) projects, part of the Italian National Antarctic Research Program (PNRA). Special thanks go to Arturo De Alteris, Massimo De Stefano, Massimiliano Esposito and Giovanni Zambardino who provided essential support to data acquisition, as well as to the captain, officers, and crew of the research vessels used for XBT launches. The authors are particularly grateful to the ESSD referees and editors for the constructive comments and suggestions provided during the manuscript discussion.

459

460

References

461

Armour, K.C., Marshall, J., Scott, J.R., Donohoe, A. and Newsom, E.R.: Southern Ocean warming delayed by circumpolar upwelling and equatorward transport, *Nat. Geosci.*, 9, 549–554, <https://doi.org/10.1038/ngeo2731>, 2016.

466

Aulicino, G. and Wadhams, P.: Editorial for the Special Issue “Remote Sensing of the Polar Oceans”. *Remote Sens.*, 14, 6195, <https://doi.org/10.3390/rs14246195>, 2022.

469

Aulicino, G., Cotroneo, Y., de Ruggiero, P., Buono, A., Corcione, V., Nunziata, F., Fusco, G.: Remote Sensing Applications in Satellite Oceanography, In P. Daponte et al. (eds.), *Measurement for the Sea*, Springer Series in Measurement Science and Technology, http://dx.doi.org/10.1007/978-3-030-82024-4_8, 2022.

474

Aulicino, G., Cotroneo, Y., and Ferola, A. I.: XBT water column temperature data collected in the Southern Ocean between New Zealand and the Ross Sea during the austral summers from 1994/1995 to 2023/2024 [Data set]. Zenodo, <https://doi.org/10.5281/zenodo.14848849>, 2025.

478

Bailey, R., Gronell, A., Phillips, H., Tanner, E., and Meyers, G.: Quality control cookbook for XBT data, Version 1.1. CSIRO Marine Laboratories Reports, 221, <https://doi.org/10.25607/OBP-1482>, 1994.

482

Belkin, I. M. and Gordon, A. L.: Southern Ocean fronts from the Greenwich meridian to Tasmania, *J. Geophys. Res.*, 101, <https://doi.org/10.1029/95JC02750>, 1996.

484

485 Botnikov, V. N.: Geographical position of the Antarctic Convergence Zone in the Antarctic
 486 Ocean, Soviet Antarctic Exped. Inform. Bull., 41, 324-327, 1963.

488 Budillon, G. and Rintoul, S. R.: Fronts and upper ocean thermal variability south of New Zealand,
 489 Antartct. Sci., 15, 141-152, <https://doi.org/10.1017/S0954102003001135>, 2003.

491 Buongiorno Nardelli, B., Guinehut, S., Verbrugge, N., Cotroneo, Y., Zambianchi, E., and Iudicone,
 492 D.: Southern Ocean mixed-layer seasonal and interannual variations from combined satellite and in
 493 situ data, J. Geophys. Res.: Oceans, 122(12), <https://doi.org/10.1002/2017JC013314>, 2017.

495 Buongiorno Nardelli, B.: A Deep Learning Network to Retrieve Ocean Hydrographic Profiles from
 496 Combined Satellite and In Situ Measurements, Remote Sens., 12, 3151.
 497 <https://doi.org/10.3390/rs12193151>, 2020.

499 Cerrone, D., Fusco, G., Cotroneo, Y., Simmonds, I., and Budillon, G.: The Antarctic circumpolar
 500 wave: Its presence and interdecadal changes during the last 142 years, J. Climate, 30(16), 6371–6389,
 501 <https://doi.org/10.1175/JCLI-D-16-0646.1>, 2017a.

503 Cerrone, D., Fusco, G., Simmonds, I., Aulicino, G., and Budillon, G.: Dominant covarying climate
 504 signals in the Southern Ocean and Antarctic sea ice influence during the last three decades. J. Climate,
 505 30(8), 3055–3072, <https://doi.org/10.1175/JCLI-D-16-0439.1>, 2017b.

507 Chelton, D. B., Schlax, M. G., Samelson, R. M.: Global observations of nonlinear mesoscale eddies,
 508 Prog. Oceanogr., Volume 91, Issue 2, 167-216, <https://doi.org/10.1016/j.pocean.2011.01.002>, 2011.

510 Chen, Z., Wang, X., Cao, H., Song, X.: Mapping high-resolution surface current by incorporating
 511 geostrophic equilibrium with surface quasigeostrophic theory using multi-source satellite
 512 observations, Remote Sens. Environ., 304, <https://doi.org/10.1016/j.rse.2024.114058>, 2024.

514 Chen, X., Chen, G., Ge, L., Cao, C. and Huang, B.: Medium-range forecasting of oceanic eddy
 515 trajectory, Int. J. Digit. Earth, 17:1, <https://doi.org/10.1080/17538947.2023.2300325>, 2024.

517 Cheng, L., J. Zhu, R. Cowley, T. Boyer, and S. Wijffels: Time, probe type, and temperature variable
 518 bias corrections to historical expendable bathythermograph observations. J. Atmos. Oceanic
 519 Technol., 31, 1793-1825, <https://doi.org/10.1175/Jtech-D-13-00197.1>, 2014.

521 Cheng, L., Abraham, J., Goni, G., Boyer, T., et al.: XBT Science: assessment of instrumental biases
 522 and errors, Bulletin of the American Meteorological Society, 97, 924-933.
 523 <http://dx.doi.org/10.1175/BAMS-D-15-00031>, 2016.

525 Convey, P., and Peck, L. S.: Antarctic environmental change and biological responses, Sci. Adv.,
 526 <https://doi.org/10.1126/sciadv.aaz0888>, 2019.

528 Cotroneo, Y., Budillon, G., Fusco, G. and Spezie, G.: Cold core eddies and fronts of the Antarctic
 529 Circumpolar Current south of New Zealand from in situ and satellite data, J. Geophys. Res.
 530 Oceans, 118, 2653–2666, <https://doi.org/10.1002/jgrc.20193>, 2013.

532

533 Cotroneo, Y., Aulicino, G., Ruiz, S., Pascual, A., Budillon, G., Fusco, G., and Tintoré, J.: Glider and
534 satellite high resolution monitoring of a mesoscale eddy in the Algerian basin: Effects on the mixed
535 layer depth and biochemistry, *J. Mar. Syst.*, 162, 73-88,
536 <https://doi.org/10.1016/j.jmarsys.2015.12.004>, 2016.
537

538 Cotroneo, Y., Budillon, G., Artegiani, A., Conversano, F., Corbo, C., Gallarato, A., et al.: Water
539 temperature data from XBT taken from the research vessel *Italica* in the Southern Ocean and
540 Southwest Pacific Ocean from 1994-11-03 to 1995-01-01 (NCEI Accession 0170608), NOAA
541 National Centers for Environmental Information. <https://doi.org/10.7289/v5rf5s9v>, 2018a.
542

543 Cotroneo, Y., Budillon, G., Artegiani, A., Conversano, F., Corbo, C., Gallarato, A., et al.: Water
544 temperature data from XBT taken from the research vessel *Italica* in the Southern Ocean and
545 Southwest Pacific Ocean from 1995-01-06 to 1995-03-02 (NCEI Accession 0170765), NOAA
546 National Centers for Environmental Information. <https://doi.org/10.7289/v53r0r5z>, 2018b.
547

548 Cotroneo, Y., Budillon, G., Artegiani, A., Ferrara, C., Meloni, R., & Spezie, G.: Water temperature
549 from XBT taken from research vessel *Italica* in the Southern Ocean and Southwest Pacific Ocean
550 from 1996-01-07 to 1996-02-18 (NCEI Accession 0171481), NOAA National Centers for
551 Environmental Information. <https://doi.org/10.7289/v5x065b9>, 2018c.
552

553 Cotroneo, Y., Budillon, G., Conversano, F., Ferrara, C., & Spezie, G.: Water temperature from XBT
554 taken from the research vessel *Italica* in the Southern Ocean and Southwest Pacific Ocean from 1997-
555 01-26 to 1997-02-19 (NCEI Accession 0172042), NOAA National Centers for Environmental
556 Information. <https://doi.org/10.7289/v5kd1w6b>, 2018d.
557

558 Cotroneo, Y., Budillon, G., Bergamasco, A., Capello, M., De Stefano, M., Ferrara, C., et al.: Water
559 temperature data from XBT collected from research vessel *Italica* in Southern Ocean and Southwest
560 Pacific Ocean from 1997-11-23 to 1998-03-06 (NCEI Accession 0172859). NOAA National Centers
561 for Environmental Information. <https://doi.org/10.7289/v50863mf>, 2018e.
562

563 Cotroneo, Y., Budillon, G., Ferrara, C., Meloni, R., Paschini, E., & Spezie, G.: Water temperature
564 from XBT taken from the research vessel *Italica* in the Southern Ocean and Southwest Pacific Ocean
565 from 1999-01-05 to 1999-01-11 (NCEI Accession 0173211), NOAA National Centers for
566 Environmental Information. <https://doi.org/10.7289/v5mg7mtc>, 2018f.
567

568 Cotroneo, Y., Budillon, G., Ferrara, C., Paschini, E., Russo, A., & Spezie, G.: Water temperature from
569 XBT taken from the research vessel *Italica* in the Southern Ocean and Southwest Pacific Ocean from
570 2000-01-07 to 2000-02-18 (NCEI Accession 0173212), NOAA National Centers for Environmental
571 Information. <https://doi.org/10.7289/v56d5r8p>, 2018g.
572

573 Cotroneo, Y., Budillon, G., Bergamasco, A., De Stefano, M., Ferrara, C., Paschini, E., & Spezie, G.:
574 Water temperature from XBT taken from the research vessel *Italica* in the Southern Ocean and
575 Southwest Pacific Ocean from 2001-01-06 to 2001-02-26 (NCEI Accession 0173213), NOAA
576 National Centers for Environmental Information. <https://doi.org/10.7289/v5s75dpg>, 2018h.
577

578 Cotroneo, Y., Budillon, G., Ferrara, C., Orsi, M., Paschini, E., Rivaro, P., & Spezie, G.: Water
579 temperature from XBT taken from the research vessel *Italica* in the Southern Ocean and Southwest
580 Pacific Ocean from 2001-12-24 to 2001-12-31 (NCEI Accession 0173214), NOAA National Centers
581 for Environmental Information. <https://doi.org/10.7289/v5ng4nzt>, 2018i.

582

583 Cotroneo, Y., Budillon, G., Bergamasco, A., De Alteris, A., De Stefano, M., Ferrara, C., et al.: Water
584 temperature from XBT taken from the research vessel *Italica* in the Southern Ocean and Southwest
585 Pacific Ocean from 2003-01-06 to 2003-01-11 (NCEI Accession 0173338), NOAA National Centers
586 for Environmental Information. <https://doi.org/10.7289/v5qz289c>, 2018j.

587

588 Cotroneo, Y., Budillon, G., Ferrara, C., Monteduro, R., Russo, A., & Spezie, G.: Water temperature
589 from XBT taken from the research vessel *Italica* in the Southern Ocean and Southwest Pacific Ocean
590 from 2003-12-24 to 2003-12-28 (NCEI Accession 0173328), NOAA National Centers for
591 Environmental Information. <https://doi.org/10.7289/v5vq3113>, 2018k.

592

593 Cotroneo, Y., Budillon, G., Aliani, S., Capello, M., Ferrara, C., Paschini, E. & Spezie, G.: Water
594 temperature from XBT taken from the research vessel *Italica* in the Southern Ocean and Southwest
595 Pacific Ocean from 2005-01-01 to 2005-01-06 (NCEI Accession 0173533), NOAA National Centers
596 for Environmental Information. <https://doi.org/10.7289/v5vh5m45>, 2018l.

597

598 Cotroneo, Y., Budillon, G., Ferrara, C., Meloni, R., & Spezie, G.: Water temperature from XBT taken
599 from the research vessel *Italica* in the Southern Ocean and Southwest Pacific Ocean from 2007-02-
600 05 to 2007-02-10 (NCEI Accession 0174709). Version 1.1, NOAA National Centers for
601 Environmental Information. <https://doi.org/10.25921/c8bm-xh74>, 2018m.

602

603 Cotroneo, Y., Budillon, G., Aliani, S., Ferrara, C., Greco, A., Meloni, R. & Spezie, G.: Water
604 temperature from XBT taken from the research vessel *Italica* in the Southern Ocean and Southwest
605 Pacific Ocean from 2008-01-16 to 2008-01-21 (NCEI Accession 0174711), Version 1.1. NOAA
606 National Centers for Environmental Information. <https://doi.org/10.25921/q29v-c980>, 2018n.

607

608 Cotroneo, Y., Budillon, G., Meloni, R., Aliani, S., Zambardino, G., & Spezie, G.: Water temperature
609 data from XBT taken from research vessel *Italica* in the Southern Ocean and Southwest Pacific Ocean
610 from 2010-01-25 to 2010-01-29 (NCEI Accession 0167835), NOAA National Centers for
611 Environmental Information. <https://doi.org/10.7289/v50r9mmm>, 2017a.

612

613 Cotroneo, Y., Budillon, G., Castagno, P., De Alteris, A., De Stefano, M., Falco, P., et al.: Water
614 temperature from XBT taken from research vessel *Italica* in the Southern Ocean and Southwest
615 Pacific Ocean from 2012-01-13 to 2012-01-19 (NCEI Accession 0167834). NOAA National Centers
616 for Environmental Information. <https://doi.org/10.7289/v54j0cbw>, 2017b.

617

618 Cotroneo, Y., Budillon, G., Castagno, P., Colizza, E., Cotterle, D., Falco, P., et al.: Water temperature
619 from XBT taken from the research vessel *Araon* in the Southern Ocean and Southwest Pacific Ocean
620 from 2013-01-24 to 2013-02-06 (NCEI Accession 0174794). Version 1.1, NOAA National Centers
621 for Environmental Information. <https://doi.org/10.25921/9YTS-P771>, 2018o.

622

623 Cotroneo, Y., Budillon, G., Falco, P., Fusco, G., et al.: Water temperature from XBT taken from the
624 research vessel *Italica* in the Southern Ocean and Southwest Pacific Ocean from 2006-01-01 to 2006-
625 01-04 (NCEI Accession 0207044). NOAA National Centers for Environmental Information.
626 <https://doi.org/10.25921/hzcp-d813>, 2019.

627

628 Cotroneo, Y., Ferola, A.I., Aulicino, G., Castagno, P. et al.: Water temperature taken by XBT from
629 the research vessel *Italica* in the Southern Ocean (> 60 degrees South) and Southwest Pacific Ocean
630 (limit-147 E to 140 W) from 2013-12-30 to 2014-02-18 (NCEI Accession 0287161). NOAA National
631 Centers for Environmental Information. <https://doi.org/10.25921/220j-b370>, 2024a.

632

633 Cotroneo, Y., Ferola, A.I., Aulicino, G., Castagno, P. et al.: Water temperature taken by XBT from
634 the research vessel *Araon* in the Southern Ocean (> 60 degrees South) and Southwest Pacific Ocean
635 (limit-147 E to 140 W) from 2015-01-02 to 2015-01-10 (NCEI Accession 0287162). NOAA National
636 Centers for Environmental Information. <https://doi.org/10.25921/9ph6-c102>, 2024b.

637

638 Cotroneo, Y., Ferola, A.I., Aulicino, G., Castagno, P. et al.: Water temperature taken by XBT from
639 the research vessel *Italica* in the Southern Ocean (> 60 degrees South) and Southwest Pacific Ocean
640 (limit-147 E to 140 W) from 2016-01-16 to 2016-01-28 (NCEI Accession 0287159). NOAA National
641 Centers for Environmental Information. <https://doi.org/10.25921/zf04-ch06>, 2024c.

642

643 Cotroneo, Y., Ferola, A.I., Aulicino, G., Castagno, P. et al.: Water temperature taken by XBT from
644 the research vessel *Italica* in the Southern Ocean (> 60 degrees South) and Southwest Pacific Ocean
645 (limit-147 E to 140 W) from 2016-12-31 to 2017-01-05 (NCEI Accession 0287163). NOAA National
646 Centers for Environmental Information. <https://doi.org/10.25921/vvmp-rr55>, 2024d.

647

648 Cotroneo, Y., Ferola, A.I., Aulicino, G., Castagno, P. et al.: Water temperature taken by XBT from
649 the research vessel *Araon* in Southern Oceans (> 60 degrees South) and Southwest Pacific Ocean
650 (limit-147 E to 140 W) from 2019-02-08 to 2019-02-12 (NCEI Accession 0287554). NOAA National
651 Centers for Environmental Information. <https://doi.org/10.25921/jeee-zf77>, 2024e.

652

653 Cotroneo, Y., Ferola, A.I., Aulicino, G., Castagno, P. et al.: Water temperature taken by XBT from
654 the research vessel *Laura Bassi* in the Southern Ocean (> 60 degrees South) and Southwest Pacific
655 Ocean (limit-147 E to 140 W) from 2020-01-07 to 2020-01-12 (NCEI Accession 0287549). NOAA
656 National Centers for Environmental Information. <https://doi.org/10.25921/1ysg-dw94>, 2024f.

657

658 Cotroneo, Y., Ferola, A.I., Aulicino, G., Castagno, P. et al.: Water temperature taken by XBT from
659 the research vessel *Laura Bassi* in the Southern Ocean (> 60 degrees South) and Southwest Pacific
660 Ocean (limit-147 E to 140 W) from 2020-12-25 to 2021-01-02 (NCEI Accession 0297164). NOAA
661 National Centers for Environmental Information. <https://doi.org/10.25921/aeg5-hw87>, 2024g.

662

663 Cotroneo, Y., Ferola, A.I., Aulicino, G., Castagno, P. et al.: Water temperature taken by XBT from
664 the research vessel *Laura Bassi* in the Southern Ocean (> 60 degrees South) and Southwest Pacific
665 Ocean (limit-147 E to 140 W) from 2022-01-08 to 2022-01-26 (NCEI Accession 0297165). NOAA
666 National Centers for Environmental Information. <https://doi.org/10.25921/3mmd-tj60>, 2024h.

667

668 Cotroneo, Y., Ferola, A.I., Aulicino, G., Castagno, P. et al.: Water temperature taken by XBT from
669 the research vessel Laura Bassi in the Southern Ocean (> 60 degrees South) and Southwest Pacific
670 Ocean (limit-147 E to 140 W) from 2023-01-06 to 2023-01-12 (NCEI Accession 0297163). NOAA
671 National Centers for Environmental Information. <https://doi.org/10.25921/kte7-d058>, 2024i.

672

673 Cotroneo, Y., Ferola, A.I., Aulicino, G., Castagno, P. et al.: Water temperature taken by XBT from
674 the research vessel Laura Bassi in the Southern Ocean (> 60 degrees South) and Southwest Pacific
675 Ocean (limit-147 E to 140 W) from 2024-01-07 to 2024-01-12 (NCEI Accession 0297166). NOAA
676 National Centers for Environmental Information. <https://doi.org/10.25921/jc13-ek97>, 2024l.

677

678 Cowley, R., Wijffels, S., Cheng, L., Boyer, T. and Kizu, S.: Biases in expendable bathythermograph
679 data: A new view based on historical side-by-side comparisons. *J. Atmos. Oceanic Technol.*, 30,
680 1195–1225, <https://doi.org/10.1175/JTECH-D-12-00127.1>, 2013.

681

682 Cowley, R. and Krummel, L. Australian XBT Quality Control Cookbook Version 2.1 (updated
683 August 2023). CSIRO, Australia. <https://doi.org/10.25919/3tm5-zn80>, 2022.

684

685 Daneshzadeh, Y.H., Festa, J.F. and Minton, S.M.: Procedures used at AOML to quality control real
686 time XBT data collected in the Atlantic Ocean. Miami, USA, NOAA Atlantic Oceanographic and
687 Meteorological Laboratory, 44pp, <https://doi.org/10.25607/OBP-1485>, 1994.

688

689 Downes, S.M., Farneti, R., Uotila, P., Griffies, S.M., Marsland, S.J. et al.: An assessment of Southern
690 Ocean water masses and sea ice during 1988–2007 in a suite of interannual CORE-II simulations,
691 *Ocean Model.*, 94, 67–94, <https://doi.org/10.1016/j.ocemod.2015.07.022>, 2015.

692

693 Falco, P. and Zambianchi, E.: Near-surface structure of the Antarctic Circumpolar Current derived
694 from World Ocean Circulation Experiment drifter data, *J. Geophys. Res. Oceans*, 116(C5),
695 <https://doi.org/10.1029/2010JC006349>, 2011.

696

697 Falco, P., Aulicino, G., Castagno, P., Capozzi, V., de Ruggiero, P., Garzia, A., Ferola, A.I., Cotroneo,
698 Y., Colella, A., Fusco, G., Pierini, S., Budillon, G., Zambianchi, E., Spezie, G.: Ocean-atmosphere-
699 ice processes in the Ross Sea: A review, *Deep Sea Research Part II: Topical Studies in Oceanography*,
700 218, 105429, <https://doi.org/10.1016/j.dsr2.2024.105429>, 2024.

701

702 Falco, P., Castagno, P., Cotroneo, Y., Aulicino, G., Budillon, G., de Ruggiero, P., Fusco, G. and
703 Zambianchi, G.: Measurements for Oceanography. In P. Daponte et al. (eds.), *Measurement for the*
704 *Sea*, Springer Series in Measurement Science and Technology, http://dx.doi.org/10.1007/978-3-030-82024-4_3, 2022.

705

706

707 Ferola, A. I., Cotroneo, Y., Wadhams, P., Fusco, G., Falco, P., Budillon, G., and Aulicino, G.: The
708 Role of the Pacific-Antarctic Ridge in Establishing the Northward Extent of Antarctic Sea-Ice,
709 *Geophys. Res. Lett.*, 50(10), <https://doi.org/10.1029/2023GL104373>, 2023.

710

711 Frenger, I., Münnich, M., Gruber, N., and Knutti, R.: Southern Ocean eddy phenomenology, *J.*
712 *Geophys. Res. Oceans*, 120, 7413–7449, <https://doi.org/10.1002/2015JC011047>, 2015.

713

714 GEBCO Compilation Group: GEBCO 2023 Grid, <https://doi.org/10.5285/f98b053b-0cbc-6c23-e053-6c86abc0af7b>, 2023.

715

716

717 Gille, S. T.: Mean sea surface height of the Antarctic Circumpolar Current from GEOSAT 600 data:
 718 methods and application, *J. Geophys. Res.*, 99, 18255-18273, <https://doi.org/10.1029/94JC01172>,
 719 1994.

720

721 Goni, G., and coauthors: More than 50 years of successful continuous temperature section
 722 measurements by 943 the global expendable bathythermograph network, its integrability, societal
 723 benefits, and future. *Front. Mar. Sci.*, 6:452, <https://doi.org/10.3389/fmars.2019.00452>, 2019.

724

725 Gouretski, V. and Reseghetti, F.: On depth and temperature biases in bathythermograph data:
 726 Development of a new correction scheme based on analysis of a global ocean database. *Deep-Sea*
 727 *Res. I*, 57, 812–833, <https://doi.org/10.1016/j.dsr.2010.03.011>, 2010.

728

729 Green, A. W.: Bulk dynamics of the expendable bathythermograph (XBT). *Deep-Sea Res.*, 31A, 415–
 730 426, [https://doi.org/10.1016/0198-0149\(84\)90093-1](https://doi.org/10.1016/0198-0149(84)90093-1), 1984.

731

732 Hanawa, K., Rual, P., Bailey, R., Sy, A., and Szabados, M.: A new depth-time equation for Sippican
 733 or TSK T-7, T-6 and T-4 expendable bathythermographs (XBT), *Deep-Sea Res. I*, 42(8), 1423-1451,
 734 [https://doi.org/10.1016/0967-0637\(95\)97154-Z](https://doi.org/10.1016/0967-0637(95)97154-Z), 1995.

735

736 Intergovernmental Oceanographic Commission (2013) Ocean Data Standards Volume 3.
 737 Recommendation for a Quality Flag Scheme for the Exchange of Oceanographic and Marine
 738 Meteorological Data. Paris, France, UNESCO-IOC, 5pp. & Annexes. Intergovernmental
 739 Oceanographic Commission Manuals and Guides, Vol. 54(3). <http://dx.doi.org/10.25607/OBP-6>.

740

741 Legler, D.M., Freeland, H.J., Lumpkin, R., Ball, G., McPhaden, M.J., North, S., Crowley, R., Goni,
 742 G.J., Send, U., and Merrifield, M.A.: The current status of the real-time in situ Global Ocean
 743 Observing System for operational oceanography, *J. Oper. Oceanogr.*, 8:sup2, s189-s200,
 744 <https://doi.org/10.1080/1755876X.2015.1049883>, 2015.

745

746 McGillicuddy Jr, D. J.: Mechanisms of physical-biological-biogeochemical interaction at the oceanic
 747 mesoscale, *Ann. Rev. Mar. Sci.*, 8, 125-159, [https://doi.org/10.1146/annurev-marine-010814-](https://doi.org/10.1146/annurev-marine-010814-015606)
 748 [015606](https://doi.org/10.1146/annurev-marine-010814-015606), 2016.

749

750 Menna, M., Cotroneo, Y., Falco, P., Zambianchi, E., Di Lemma, R., Poulain, P. M. and Budillon, G.:
 751 Response of the Pacific Sector of the Southern Ocean to wind stress variability from 1995 to 2017, *J.*
 752 *Geophys. Res. Oceans*, 125(10), <https://doi.org/10.1029/2019JC015696>, 2020.

753

754 Morales Maqueda, M. A., Willmott, A. J. and Biggs, N. R. T.: Polynya dynamics: A review of
 755 observations and modelling, *Rev. Geophys.*, 42.1, <https://doi.org/10.1029/2002RG000116>, 2004.

756

757 Orsi, A. H., Whitworth, T., and Nowlin, W. D.: On the meridional extent and fronts of the Antarctic
 758 circumpolar current, *Deep-Sea Res. I*, 42(5), 641–673, [https://doi.org/10.1016/0967-0637\(95\)00021-](https://doi.org/10.1016/0967-0637(95)00021-W)
 759 [W](https://doi.org/10.1016/0967-0637(95)00021-W), 1995.

760

761 Parks, J., Bringas, F., Cowley, R., Hanstein, C., Krummel, L., Sprintall, J., Cheng, L., Cirano, M.,
 762 Cruz, S., Goes, M., Kizu, S. and Reseghetti, F.: XBT operational best practices for quality assurance,
 763 *Front. Mar. Sci.*, 9, 991760, <https://doi.org/10.3389/fmars.2022.991760>, 2022

764

765 Reverdin, G., Marin, F. Bourles, B. and L’Herminier, P.: XBT temperature errors during French
 766 research cruises (1999–2007). *J. Atmos. Oceanic Technol.*, 26, 2462–2473,
 767 <https://doi.org/10.1175/2009JTECHO655.1>, 2009.

768
769 Rintoul, S. R., Donguy, J. R., and Roemmich, D. H.: Seasonal evolution of upper ocean thermal
770 structure between Tasmania and Antarctica. *Deep-Sea Res. I*, 44(7), 1185-1202,
771 [https://doi.org/10.1016/S0967-0637\(96\)00125-2](https://doi.org/10.1016/S0967-0637(96)00125-2), 1997.
772
773 Rintoul, S. R.: The global influence of localized dynamics in the Southern Ocean, *Nature*, 558, 209–
774 218, <https://doi.org/10.1038/s41586-018-0182-3>, 2018.
775
776 Roemmich, D., Wilson, W.S., Gould, W.J., Owens, W.B., Le Traon, P.-Y., Freeland, H.J., King,
777 B.A., Wijffels, S., Sutton, P.J.H., Zilberman, N.: Chapter 4 - The Argo Program, In *Science of*
778 *Sustainable Systems, Partnerships in Marine Research*, Auad, G. and Wiese F.K. (eds), Elsevier, 53-
779 69, <https://doi.org/10.1016/B978-0-323-90427-8.00004-6>, 2022.
780
781 Schlitzer, R. Ocean Data View, <http://odv.awi.de>, 2011.
782
783 Seaver, G.A. and Kuleshov, S.: Experimental and analytical error of the expendable
784 bathythermograph. *J. Phys. Oceanogr.*, 12, 592–600, [https://doi.org/10.1175/1520-0485\(1982\)012<0592:EAAEOT.2.0.CO;2](https://doi.org/10.1175/1520-0485(1982)012<0592:EAAEOT.2.0.CO;2), 1982.
785
786 Seo, H., O'Neill, L. W., Bourassa, M. A., Czaja, A., Drushka, K., Edson, J. B., Fox-Kemper, B.,
787 Frenger, I., Gille, S. T., Kirtman, B. P., Minobe, S., Pendergrass, A. G., Renault, L., Roberts, M. J.,
788 Schneider, N., Small, R. J., Stoffelen, A., and Wang, Q.: Ocean Mesoscale and Frontal-Scale Ocean–
789 Atmosphere Interactions and Influence on Large-Scale Climate: A Review, *J. Climate*, 36(7), 1981-
790 2013. <https://doi.org/10.1175/JCLI-D-21-0982.1>, 2023.
791
792 Simoncelli, S., Reseghetti, F., Fratianni, C., Cheng, L., and Raiteri, G.: Reprocessing of eXpendable
793 BathyThermograph (XBT) profiles from the Ligurian and Tyrrhenian seas over the time period 1999–
794 2019 with a full metadata upgrade, *Earth Syst. Sci. Data*, 16, 5531–5561,
795 <https://doi.org/10.5194/essd-16-5531-2024>, 2024.
796
797 Sokolov, S. and Rintoul, S. R.: Circulation structure and distribution of the Antarctic circumpolar
798 current fronts: 2. Variability and relationship to sea surface height, *J. Geophys. Res.*, 114(C11),
799 C11019, <https://doi.org/10.1029/2008JC005248>, 2009b.
800
801 Sokolov, S. and Rintoul, S. R.: Circumpolar structure and distribution of the Antarctic Circumpolar
802 Current fronts: 1. Mean circumpolar paths, *J. Geophys. Res.*, 114(C11), C11018,
803 <https://doi.org/10.1029/2008jc005108>, 2009a.
804
805 Sokolov, S. and Rintoul, S. R.: Multiple Jets of the Antarctic Circumpolar Current South of Australia,
806 *J. Geophys. Res.*, 37, <https://doi.org/10.1175/JPO3111.1>, 2007.
807
808 Tan, Z., Cheng, L., Gouretski, V., Zhang, B., Wang, Y., Li, F. and Zhu, J.: A new automatic quality
809 control system for ocean profile observations and impact on ocean warming estimate, *Deep-Sea Res.*
810 *I*, 194, 103961, <https://doi.org/10.1016/j.dsr.2022.103961>, 2023.
811
812 Trani, M., Falco, P. and Zambianchi, E.: Near-surface eddy dynamics in the Southern Ocean, *Polar*
813 *Research*, 30(1), 11203. <https://doi.org/10.3402/polar.v30i0.11203>, 2011.
814
815 Trani, M., Falco, P., Zambianchi, E., and Saltee, J. B.: Aspects of the Antarctic Circumpolar Current
816 dynamics investigated with drifter data, *Prog. Oceanogr.*, 125, 1–15,
817 <https://doi.org/10.1016/j.pocean.2014.05.001>, 2014.
818